Preparation of a steady entangled state of two nitrogen-vacancy centers by simultaneously utilizing two dissipative factors

Zhao Jin

Department of Physics, College of Sciences, Northeastern University, Shenyang 110819, China

S. L. Su [*]

School of Physics, Zhengzhou University, Zhengzhou 450001, China

Shou Zhang[†]

Department of Physics, Harbin Institute of Technology, Harbin 150001, China
and Department of Physics, College of Science, Yanbian University, Yanji, Jilin 133002, China

A dissipation-based scheme is proposed to prepare the steady entangled state of two spatially separated nitrogen-vacancy (NV) centers fixed on the exterior surface of two microtoroidal resonators coupled by a whispering-gallery-mode (WGM) field. The effective operator method is used to get an effective master equation which simplifies the systematic dynamics into ground-state subspace. Based on the effective dynamics, the parameter condition to use the NV center's spontaneous emission and that to use the resonator's photon loss as resources to prepare entanglement are achieved. Interestingly, we find that these two conditions are almost the same. To some extent, these two dissipative factors are no longer detrimental, but can be used simultaneously as powerful resources to prepare the steady entangled state, which forms a sharp contrast with most of the currently schemes utilizing one dissipative factor. On the other hand, the different forms of the steady entangled state are achievable via modulating systematic parameters. The scheme is independent of initial states and does not require precise time control. Numerical results show that high fidelity and purity can be obtained and the scheme is robust against small parameter deviations.

I. INTRODUCTION

Dissipation has been considered a detrimental factor traditionally because it would destroy unitary dynamics and induces errors. The quest to find viable strategies for mitigating errors is an essential prerequisite for the development of quantum technologies. Generally, a variety of feasible methods have been devised, including quantum error correction [1,2], decoherence-free subspaces (DFSs) [3–5], and noiseless subsystems [6,7]. Recently, a new opinion has been put forward: the dissipation can act as a resource for quantum information processing, in cases such as universal quantum computation [8], quantum repeaters [9], quantum memories [10], and quantum simulators [11,12] within the framework of quantum reservoir engineering. Moreover, the dissipation also provides a means of quantum entangled state preparation for atom-cavity and solid state systems [11,13–28] and for quantum computation [8,29]. In contrast to unitary-dynamics-based schemes, these dissipation-based schemes to prepare quantum entangled states do not require specifying initial states and controlling evolution time accurately, and the prepared entangled state is the steady state of the system.

In particular, Kastoryano *et al.* consider a dissipative scheme for preparing a maximally entangled state of two Λ atoms in a high finesse optical cavity [15] based on the effective operator method developed by the same group [17] and widely used in Refs. [17–21]. In addition, a scheme for the dissipative preparation of specific entangled states between two nitrogen-vacancy (NV) centers was also proposed [22]. Moreover, Zheng *et al.* proposed a scheme to prepare the maximal entanglement between two atoms coupled to a decaying resonator [23]. These schemes in Refs. [22,23] show that the resonator's photon loss plays a positive role in state preparation. Nevertheless, the NV center's and atomic spontaneous emission would decrease the performance of the schemes. Differently, Ref. [20] shows that atomic spontaneous emission can also to be used to prepare the entangled state but cavity mode leakage plays negative roles. Busch *et al.* show that both dissipative factors can be utilized to cool the system to an entangled state but more classical lasers are required [16]. And almost all of the dissipation-based schemes are aiming to prepare one specific entangled state.

Although many quantum computing schemes are based on photon [30], ion [31], and atom [32–34] systems, solid-state-based quantum platforms such as quantum dots [35], superconducting circuits [36], or color centers are also given much attention due to the scalable property of quantum information processing (QIP). Particularly, the NV center

_____

[*]slsu@zzu.edu.cn
[†]szhang@ybu.edu.cn

consisting of a substitutional nitrogen atom and an adjacent vacancy in diamond has been considered as an excellent candidate for QIP [37]. Many fundamental researches confirm that electron spin states in NV centers have a long lifetime even at room temperature and can be manipulated by an electromagnetic field or optical pulse [38,39]. Importantly, the NV center provides a Λ-type three-level system [40–42], which can be used for various quantum engineering applications. As a promising application, the combination of NV centers and microcavities has gained widespread attention [43–47]. One of the microcavities is the microtoroidal resonator (MTR) with a quantized whispering-gallery-mode (WGM) which exhibits ultrahigh quality factor and small mode volume [48–51]. Many QIP tasks have been proposed to be accomplished by means of NV centers coupled with WGM microresonators, such as entangled state generation [52], quantum state transfer [53], conditional phase gate construction[54], and distributed QIP by coupling the two cavities via either a flying photon or optical-fiber-taper waveguide [22,55].

In addition, the NV center can also offer heterogeneous spin degrees of freedom where the bound electron spins are used for fast high-fidelity control and readout [56,57] while the nearby nuclear spins are used as long-lived quantum bits [58,59]. Therefore, the nuclear spins have proved to be a valuable resource for nonvolatile memory [60] via hyperfine interaction between electron and nuclear spins. In Refs. [61] and [62], high-quality entanglement between two nuclear spins in diamond has been demonstrated to occur via the spin state storage technique and repeated qubit parity measurement, respectively. However, these two methods require specified initialization and precise time control. In contrast, Chen *et al.* designed a dissipative scheme [63] to generate a high-fidelity singlet pair of nuclear spins, in which the final state is independent of the initial state of the nuclei and robust to external field fluctuations. Similarly, Ref. [64] showed that the decay of short-lived electron spins in solids can be exploited to generate an entangled steady state between electron and nuclear spins for any initial state conditions. It is interesting to compare this protocol with Ref. [63]. The main idea in Ref. [63] is the combination of periodic resets of the electron spin which provides a tunable artificial reservoir and coherent local control of the target nuclear spins with imbalanced detunings to ensure that the steady singlet state of the nuclei is unique. In contrast, Ref. [64] is based on the dark state interference effects of the optical and microwave driving fields in the presence of spontaneous emission from the electronic excited states to stabilize the maximally entangled state of the electron and nuclear spins.

In this work, based on the effective operator method [17], we propose a scheme for dissipative preparation of an electronic steady entangled state of two spatially separated NV centers; especially, the steady maximally entangled Knill-Laflamme-Milburn (KLM) [65] state, which plays important roles in QIP, such as quantum teleportation [66] and quantum error correction [67]. In order to know more clearly the effect of each dissipative factor, we first consider the system without spontaneous emission of NV centers and then consider it without resonator decay. Interestingly, we find that the conditions for achieving the dominant dissipative channels of

the spontaneous-emission-based case are exactly consistent with those of the resonator-decay-based case, which means that our proposal can take advantage of both dissipation factors simultaneously. Our scheme forms sharp contrast to the schemes [15,18,20,23] in which one out of the two factors plays a positive role while the other plays a negative role.

The main characteristics of our scheme can be summarized as follows: (i) Both spontaneous emission of NV centers and resonator decay can be utilized simultaneously for preparing the entangled state. (ii) The different forms of the steady entangled state can be achieved by modulating the detuning (β) and effective Rabi frequency (Ω_L) of the classical field, which lead to the diversity of the prepared entangled states and would no doubt broaden the applications of the scheme. (iii) Unlike the dissipation-based scheme studied in the atom-cavity system [15,19,23,24], our scheme considers the solid-state system, which has advantages in storing quantum information and repetitive readout. (iv) In contrast to the unitary-dynamics-based scheme, it does not require specifying the initial state and accurately controlling the evolution time.

This paper is organized as follows. In Sec. II, we describe the model Hamiltonian and derive the effective dynamics of the system. In Secs. III A and III B, we prepare steady entangled states by only utilizing resonator decay and spontaneous emission of NV centers, respectively. In Sec. III C, we simultaneously consider the two dissipative factors to prepare the steady entangled state and numerically simulate the fidelity of the target steady state with different entanglement forms via modulating systematic parameters Ω_L and β. In Sec. IV, we consider the experimental implementation and the robustness. The conclusions are summarized in Sec. V.

II. BASIC MODEL

The negatively charged NV center has six electrons from the nitrogen and three carbons surrounding the vacancy. The electron-spin ground states of an NV center consist of a spin triplet labeled as $|^3A_2\rangle$ with 2.88 GHz splitting between the lower $|m_s = 0\rangle$ level and the upper levels $|m_s = \pm1\rangle$ due to the spin-spin interactions [70]. The structures of six excited states are defined by group theory [42]: $|A_1\rangle = (|E_-\rangle|m_s = +1\rangle - |E_+\rangle|m_s = -1\rangle)/\sqrt{2}$, $|A_2\rangle = (|E_-\rangle|m_s = +1\rangle + |E_+\rangle|m_s = -1\rangle)/\sqrt{2}$, $|E_x\rangle = |X\rangle|m_s = 0\rangle$, $|E_y\rangle = |Y\rangle|m_s = 0\rangle$, $|E_1\rangle = (|E_-\rangle|m_s = -1\rangle - |E_+\rangle|m_s = +1\rangle)/\sqrt{2}$, and $|E_2\rangle = (|E_-\rangle|m_s = -1\rangle + |E_+\rangle|m_s = +1\rangle)/\sqrt{2}$. Here, $|E_\pm\rangle$, $|X\rangle = (|E_-\rangle - |E_+\rangle)/2$, and $|Y\rangle = i(|E_-\rangle + |E_+\rangle)/2$ are the orbital states, and $|E_\pm\rangle$ has angular momentum projections ±1 along the NV axis. It is known [42,71] that the spin-spin interaction splits the states $|A_1\rangle$ and $|A_2\rangle$ by ~3.3 GHz. The spin-orbit interaction produces different total angular momenta among the pairs (A_1, A_2), (E_x, E_y), and (E_1, E_y) which are split from each other by about 5.5 GHz. Thus, the state $|A_2\rangle$ is robust to low strain and magnetic fields due to the stable symmetric properties that are protected by an energy gap arising from the spin-orbit and spin-spin interactions. And it decays to the ground-state sublevels $|m_s = +1\rangle$ and $|m_s = -1\rangle$ with radiation of σ^- and σ^+ circular polarizations, respectively [42,55]. The σ^- (σ^+) corresponds to the right(left)-circularly polarized light. This particularly useful Λ-type transition was employed
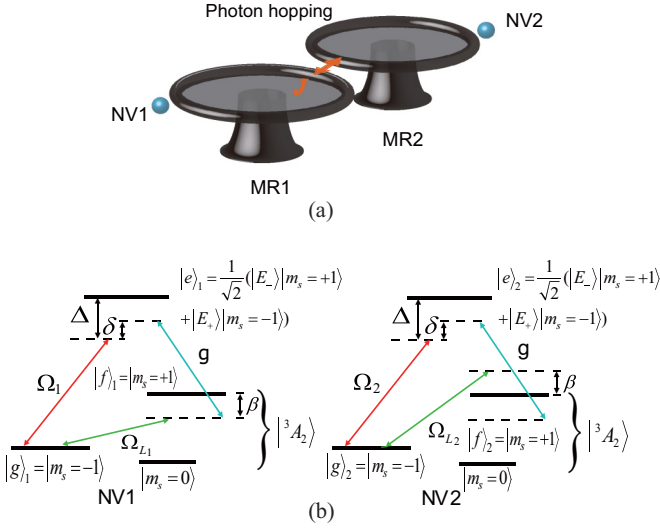
FIG. 1. (a) The schematic for dissipative preparation of a steady entangled state between two NV centers coupled to two different MTRs, respectively. The MTRs are coupled via evanescent fields of the WGM. (b) Energy level structure of two NV centers. Quantum information is encoded in the spin states $|m_s = \pm 1\rangle$ of the $^3A_2$ triplet, i.e., $|g\rangle_i \equiv |m_s = -1\rangle$ and $|f\rangle_i \equiv |m_s = +1\rangle$ ($i = 1, 2$). The excited state is $|e\rangle_i \equiv 1/\sqrt{2}(|E_-\rangle|m_s = +1\rangle + |E_+\rangle|m_s = -1\rangle)$. It should be mentioned that, according to the selection rule of the transitions [42,68], the ground state sublevels $|m_s = +1\rangle$ and $|m_s = -1\rangle$ cannot be coupled directly. However, the transitions $|g\rangle_{1(2)} \leftrightarrow |f\rangle_{1(2)}$ with detuning β ($-\beta$) and effective Rabi frequency $\Omega_{L_{1(2)}}$ can be achieved by the Raman process (see Appendix A) or by a stress applied perpendicularly to the axial direction of the NV center [69]. In the main text, we temporarily use the direct ground state coupling process to illustrate the scheme, while in the Appendix we give the practical correspondence of the ground state coupling based on the Raman process.

experimentally for spin-photon entanglement generation [42]. In addition, if one considers polarization of the single-photon pulse input in a MTR under the resonant regime, different phase shifts for the left-circularly and right-circularly polarized light reflected from the NV-MTR coupled system would be yielded, which is called Faraday rotation [72] and can be easily detected experimentally [73]. This giant Faraday rotation induced by a single-electron spin originates from the spin-dependent optical transitions and the effect of cavity quantum electrodynamics (QED).

In our work, we consider two negatively charged NV centers fixed on the exterior surfaces of two MTRs, which are coupled via the evanescent fields of the WGM, as shown in Fig. 1(a). The relevant electron level structures of the NV centers coupled by WGM, driving lasers, and effective classical fields are shown in Fig. 1(b). We encode the qubits as $|m_s = -1\rangle \equiv |g\rangle_i$, $|m_s = +1\rangle \equiv |f\rangle_i$, and $1/\sqrt{2}(|E_-\rangle|m_s = +1\rangle + |E_+\rangle|m_s = -1\rangle) \equiv |e\rangle_i$ ($i = 1, 2$), which facilitates quantum information storage and further applications. By combining individual laser pulse (σ^+ circularly polarized) irradiation [41,74] with the WGM field (σ^- circularly polarized), one can model each NV center as an optical Λ-type three-level structure. For the first (second) NV center, an off-resonance

coherent laser with detuning Δ and Rabi frequency $\Omega_{1(2)}$ is applied to drive the transition $|g\rangle_{1(2)} \leftrightarrow |e\rangle_{1(2)}$. The WGM dispersively couples the transition $|f\rangle_{1(2)} \leftrightarrow |e\rangle_{1(2)}$ with the detuning $\Delta - \delta$ and coupling strength g, where δ is resonator detuning from two-photon resonance.

We assume that the level splittings are the same for the two NV centers and do not fluctuate in time. Within the rotating wave approximation, the system Hamiltonian can be written as $\hat{H} = \hat{H}_0 + \hat{H}_g + \hat{V}_+ + \hat{V}_-$, where

$$
\begin{aligned}
\hat{H}_0 &= \delta(a_1^\dagger a_1 + a_2^\dagger a_2) + \Delta(|e\rangle_1\langle e| + |e\rangle_2\langle e|) \\
&+ [g(|e\rangle_1\langle f|a_1 + |e\rangle_2\langle f|a_2) + \text{H.c.}] \\
&+ J(a_1^\dagger a_2 + a_1 a_2^\dagger),
\end{aligned} \tag{1}
$$

$$
\begin{aligned}
\hat{H}_g &= \sum_{m=1,2} \frac{\Omega_{L_m}}{2}(|g\rangle_m\langle f| + \text{H.c.}) \\
&+ \beta(|f\rangle_1\langle f| - |f\rangle_2\langle f|),
\end{aligned} \tag{2}
$$

$$
\hat{V}_+ = \sum_{n=1,2} \frac{\Omega_n}{2}(|e\rangle_n\langle g| + \text{H.c.}), \tag{3}
$$

$$
\hat{V}_- = \hat{V}_+^\dagger, \tag{4}
$$

where a_j is the annihilation operator for the jth ($j = 1, 2$) resonator mode and J is the hopping rate of photons between the resonators. By introducing two delocalized bosonic modes $c_1 = (a_1 - a_2)/\sqrt{2}$, $c_2 = (a_1 + a_2)/\sqrt{2}$, the Hamiltonian $\hat{H}_0$ can be rewritten as

$$
\begin{aligned}
\hat{H}_0 &= \frac{g}{\sqrt{2}}[|e\rangle_1\langle f|(c_1 + c_2) + |e\rangle_2\langle f|(c_1 - c_2) + \text{H.c.}] \\
&+ (\delta - J)c_1^\dagger c_1 + (\delta + J)c_2^\dagger c_2 + \Delta\sum_{i=1,2}|e\rangle_i\langle e|. \tag{5}
\end{aligned}
$$

Here, $\hat{H}_0$ describes that delocalized field mode $c_{1(2)}$ interacts with the NV center asymmetrically (symmetrically) due to the contributions of the resonator modes. Thus, each of them would cause a collective dissipation channel.

We assume that the system-environment interaction is Markovian so that the temporal evolution of the system can be described by the Lindblad master equation

$$
\dot{\rho} = i[\rho, H] + \frac{1}{2}\sum_x[2\hat{\mathcal{L}}_x\hat{\rho}\hat{\mathcal{L}}_x^\dagger - (\hat{\mathcal{L}}_x^\dagger\hat{\mathcal{L}}_x\hat{\rho} + \hat{\rho}\hat{\mathcal{L}}_x^\dagger\hat{\mathcal{L}}_x)], \tag{6}
$$

where the Lindblad operators $\hat{\mathcal{L}}_x$ with x belong to the set $\{\kappa 1, \kappa 2, \gamma 1, \gamma 2, \gamma 3, \gamma 4\}$ denoted as the dissipation process of the system. We assume $\kappa_1 = \kappa_2 = \kappa$ and $\gamma_1 = \gamma_2 = \gamma$ for simplicity, and the six Lindblad operators can be expressed as $\hat{\mathcal{L}}_{\kappa 1} = \sqrt{\kappa}c_1$, $\hat{\mathcal{L}}_{\kappa 2} = \sqrt{\kappa}c_2$, $\hat{\mathcal{L}}_{\gamma 1} = \sqrt{\gamma/2}|g\rangle_1\langle e|$, $\hat{\mathcal{L}}_{\gamma 2} = \sqrt{\gamma/2}|g\rangle_2\langle e|$, $\hat{\mathcal{L}}_{\gamma 3} = \sqrt{\gamma/2}|f\rangle_1\langle e|$, and $\hat{\mathcal{L}}_{\gamma 4} = \sqrt{\gamma/2}|f\rangle_2\langle e|$ with the branching spontaneous emission rate. Under the weak excitation condition, the excited states of the NV center and the delocalized field modes can be adiabatically eliminated when the excited states are not initially populated. On that basis, one can get the effective master equation as [17]

$$
\begin{aligned}
\dot{\rho} &= i[\hat{\rho}, \hat{H}_{\text{eff}}] + \frac{1}{2}\sum_x\{2\hat{\mathcal{L}}_{\text{eff}}^x\hat{\rho}(\hat{\mathcal{L}}_{\text{eff}}^x)^\dagger - [(\hat{\mathcal{L}}_{\text{eff}}^x)^\dagger\hat{\mathcal{L}}_{\text{eff}}^x\hat{\rho} \\
&+ \hat{\rho}(\hat{\mathcal{L}}_{\text{eff}}^x)^\dagger\hat{\mathcal{L}}_{\text{eff}}^x]\}, \tag{7}
\end{aligned}
$$

where

$$\hat{H}_{\text{eff}} = -\frac{1}{2}\left[\hat{V}_-\hat{H}_{NH}^{-1}\hat{V}_+ + \hat{V}_-(\hat{H}_{NH}^{-1})^\dagger\hat{V}_+\right] + \hat{H}_g,$$
$$\hat{\mathcal{L}}_{\text{eff}}^x = \hat{\mathcal{L}}_x\hat{H}_{NH}^{-1}V_+, \qquad (8)$$

where $\hat{H}_{NH}^{-1}$ is the inverse of the non-Hermitian Hamiltonian $\hat{H}_{NH}^{-1} = \hat{H}_0 - i/2\sum_x(\hat{\mathcal{L}}_x)^\dagger\hat{\mathcal{L}}_x$.

In the following, we use the effective operator method to simplify the system and study the dissipative process. Full Hamiltonian H rather than effective Hamiltonian H_{eff} is used for numerical simulation to assess the performance of this scheme.

III. PREPARATION OF KLM-TYPE STEADY ENTANGLED STATE

A. Use delocalized field mode decay as a resource

For the sake of gaining better insight into the effect of delocalized field mode decay on the preparation of entanglement, we neglect the influence of spontaneous emission first. For simplicity, we set $\Omega_1 = \Omega_2 = \Omega$ and $\Omega_{L_1} = \Omega_{L_2} = \Omega_L$ and work in the triplet-singlet basis of the ground states: $\{|gg\rangle, |ff\rangle, |T\rangle, |S\rangle\}$, where $|gg\rangle = |g\rangle_1|g\rangle_2$, $|ff\rangle = |f\rangle_1|f\rangle_2$, $|T\rangle = 1/\sqrt{2}(|g\rangle_1|f\rangle_2 + |f\rangle_1|g\rangle_2)$, and $|S\rangle = 1/\sqrt{2}(|g\rangle_1|f\rangle_2 - |f\rangle_1|g\rangle_2)$. The effective Hamiltonian, along with the effective Lindblad operators corresponding to delocalized field mode decay, are given as Eqs. (B1)–(B5) in Appendix B.

As shown in Fig. 2(a), $\hat{\mathcal{L}}_{\text{eff}}^{\kappa_1}$ [Eq. (B3) in Appendix B] indicates the effective decays from $|gg\rangle$ to $|S\rangle$ at a rate $K_{1,1}$ and from $|S\rangle$ to $|ff\rangle$ at a rate $K_{1,2}$ caused by the c_1 mode; $\hat{\mathcal{L}}_{\text{eff}}^{\kappa_2}$ [Eq. (B4) in Appendix B] denotes the effective decays from $|gg\rangle$ to $|T\rangle$ at a rate $K_{2,1}$ and from $|T\rangle$ to $|ff\rangle$ at a rate $K_{2,2}$ caused by the c_2 mode simultaneously. The decay rates $K_{1,1(2)}$ and $K_{2,1(2)}$ are equal to the square of the first (second) coefficient on the right-hand side of Eqs. (B3) and (B4), respectively. If we set $M_{\kappa_1} = M_{\kappa_2} = 0$,

$$J = \sqrt{\delta^2 - (\delta/\Delta)g^2} \qquad (9)$$

is achieved which leads to $K_{1(2),1} \gg K_{1(2),2}$. That is, the decays from $|S\rangle$ to $|ff\rangle$ and from $|T\rangle$ to $|ff\rangle$ can both be largely suppressed. On the other hand, the effective classical fields cause resonant transitions between the three triplet states $\{|gg\rangle, |ff\rangle, |T\rangle\}$ and coherent shuffling of the states $|S\rangle$ and $|T\rangle$ with coupling strength β [Eq. (B2) in Appendix B]. The combined effect of the unitary and dissipative dynamics drives the population to singlet state $|S\rangle$ and overlap with $|ff\rangle$. It can be seen that

$$|\psi_S\rangle = \frac{1}{\sqrt{\frac{\Omega_L^2}{2}+\beta^2}}\left(\beta|ff\rangle + \frac{\Omega_L}{\sqrt{2}}|S\rangle\right) \qquad (10)$$

is the unique steady singlet-like state [75] of the master equation (7), i.e., $\hat{\rho}(t \to \infty) = |\psi_S\rangle\langle\psi_S|$. This state is equivalent to a standard KLM state [65] by applying local operations and modulating the parameters $\beta = \Omega_L/\sqrt{2}$. To understand the dissipative state preparation mechanism more clearly, we transform the dynamics of the system into the steady state
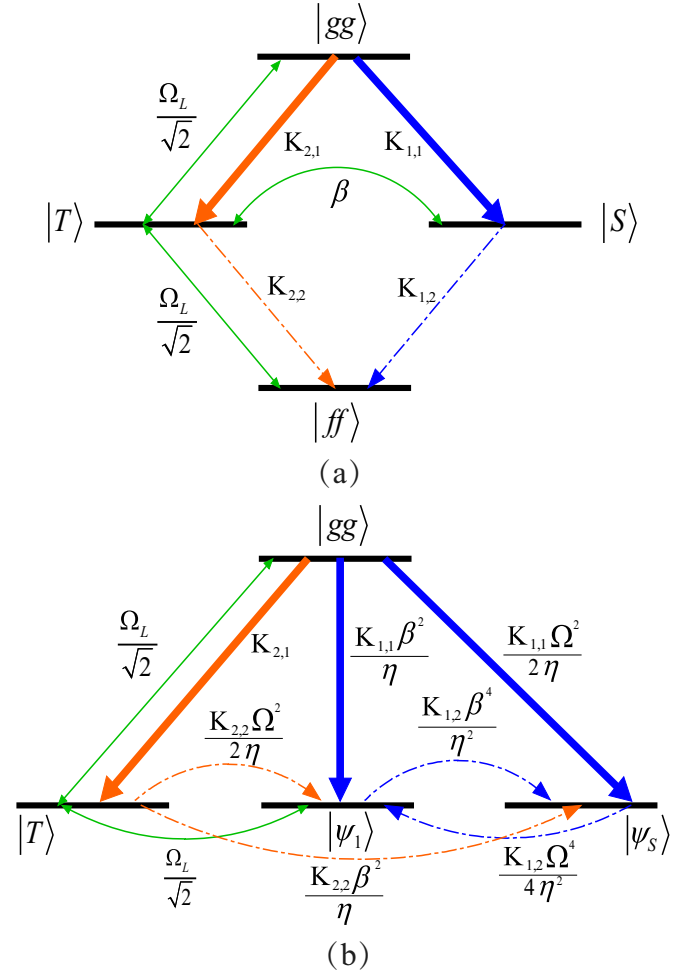

(a)

(b)

FIG. 2. Effective processes for coherent and dissipative (delocalized field modes decay) interactions. (a) In the triplet-singlet basis picture, effective classical fields cause resonant transitions between the three triplet states $\{|gg\rangle, |ff\rangle, |T\rangle\}$. The singlet state $|S\rangle$ is coherently coupled to $|T\rangle$ by the level shift β. The states of the NV center decay from $|gg\rangle$ to $|S\rangle$ and $|T\rangle$ with effective decay rates $K_{1,1}$ and $K_{2,1}$, and from $|S\rangle$ and $|T\rangle$ to $|ff\rangle$ with effective decay rates $K_{1,2}$ and $K_{2,2}$. (b) In the steady-state picture, the desired steady state $|\psi_S\rangle$ is no longer coherently coupled, but dissipatively prepared from $|gg\rangle$ at a rate of $K_{1,1}\Omega^2/2\eta$, where $\eta = \beta^2 + \Omega^2/2$.

picture consisting of $|\psi_S\rangle$ and the orthogonal state

$$|\psi_1\rangle = \frac{1}{\sqrt{\frac{\Omega_L^2}{2}+\beta^2}}\left(\frac{\Omega_L}{\sqrt{2}}|ff\rangle - \beta|S\rangle\right). \qquad (11)$$

As shown in Fig. 2(b), the desired steady state $|\psi_S\rangle$ is no longer coherently coupled, while the other three undesired states are well shuffled by effective classical fields. Under the condition $K_{1(2),1} \gg K_{1(2),2}$, the decaying processes related to $K_{1,2}$ ($|\psi_S\rangle \to |\psi_1\rangle$ and $|\psi_1\rangle \to |\psi_S\rangle$) and $K_{2,2}$ ($|T\rangle \to |\psi_1\rangle$ and $|T\rangle \to |\psi_S\rangle$) are greatly suppressed. Hence, the dissipation dynamics of the system is mainly governed by the effective decays from $|gg\rangle$ to $|\psi_S\rangle$ at a rate $K_{1,1}\Omega^2/2\eta$, from $|gg\rangle$ to $|\psi_1\rangle$ at a rate $K_{1,1}\beta^2/\eta$, and from $|gg\rangle$ to $|T\rangle$ at a rate $K_{2,1}$, where $\eta = \beta^2 + \Omega^2/2$. With the coherent drivings and delocalized field modes decay continuing, the population of
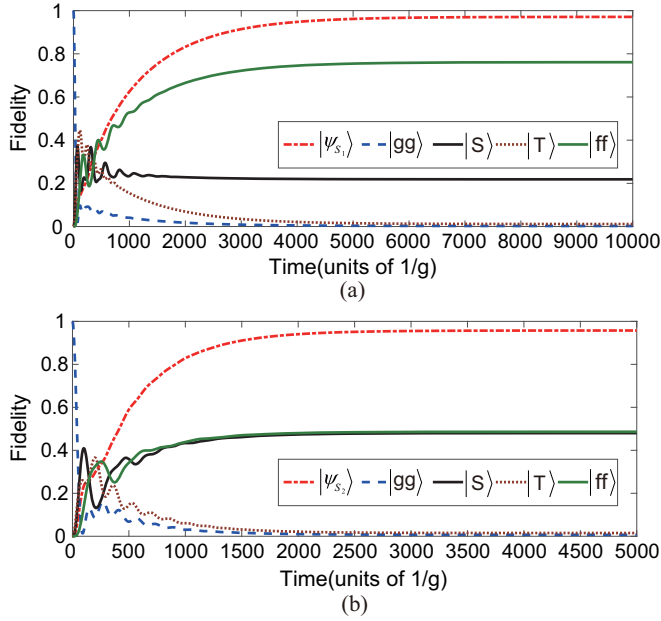
FIG. 3. (a) [(b)] Time evolution of the fidelities of target state $|\psi_{S_1}\rangle = 1/\sqrt{41}(3|S\rangle + 4\sqrt{2}|ff\rangle)$ $[|\psi_{S_2}\rangle = 1/\sqrt{2}(|ff\rangle + |S\rangle)]$, three triplet states $\{|gg\rangle, |ff\rangle, |T\rangle\}$, and singlet state $|S\rangle$ versus time in units of g^{-1} with the initial state $|gg\rangle$. In (a), the parameters are chosen as $\Omega = 0.065g$, $\Omega_L = 0.015g$, $\beta = 4\Omega_L/3$, $\Delta = 1.3g$, $\delta = 0.942g$, $J = \sqrt{\delta^2 - (\delta/\Delta)g^2}$, $\kappa = 0.06g$, and $\gamma = 0$. In (b), the parameters are chosen as $\Omega = 0.075g$, $\beta = \Omega_L/\sqrt{2}$, $\Delta = 2.2g$, $\kappa = 0.03g$, and other parameters are the same as in (a).

the desired entangled state $|\psi_S\rangle$ is gradually accumulated over time.

The preparation of the steady state is independent of the initial states. Consider the initial state $|S\rangle$ or $|ff\rangle$, which can be regarded as a superposition of the states $|\psi_1\rangle$ and $|\psi_S\rangle$. As has been shown, $|gg\rangle$, $|T\rangle$, and $|\psi_1\rangle$ can be translated to each other through effective classical fields. And $|gg\rangle$ would be transformed to $|\psi_S\rangle$ due to the combined effect of the unitary dynamics and the dissipative process. Thus the initial state $|S\rangle$ or $|ff\rangle$ would be converted to the desired state finally. Similarly, if the initial state is $|T\rangle$, it would be transformed to the state $|\psi_S\rangle$.

In order to verify the feasibility of above analysis, we numerically solve the full Lindblad master equation in Eq. (6) and utilize the definition of fidelity $F(t) \equiv \text{Tr}[(|\Phi\rangle\langle\Phi| \otimes I_c)\hat{\rho}(t)]$ $(|\Phi\rangle = |\psi_S\rangle, |gg\rangle, |\psi_S\rangle, |\psi_T\rangle,$ and $|\psi_T\rangle)$ to assess the performance of the current scheme. In Fig. 3(a) [3(b)], we consider the parameter relation $\beta = 4\Omega_L/3$ $[\beta = \Omega_L/\sqrt{2}]$ and plot the fidelity of target state $|\psi_{S_1}\rangle = 1/\sqrt{41}(3|S\rangle + 4\sqrt{2}|ff\rangle)$ $[|\psi_{S_2}\rangle = 1/\sqrt{2}(|ff\rangle + |S\rangle)]$, three triplet states $\{|gg\rangle, |ff\rangle, |T\rangle\}$, and singlet state $|S\rangle$ starting from the initial state $|gg\rangle$. We can obtain the target states $|\psi_{S_1}\rangle$ and $|\psi_{S_2}\rangle$ both with fidelities higher than 95%, and the times needed for reaching the steady state are $9065/g$ and $4560/g$, respectively. In Figs. 3(a) and 3(b), the fidelities of singlet state $|S\rangle$ (black solid line) and triplet state $|ff\rangle$ (green solid line) exhibit a distinct difference and an approximate coincidence when the system is in stabilization, respectively, which exactly characterize two forms of the steady entangled state that can be
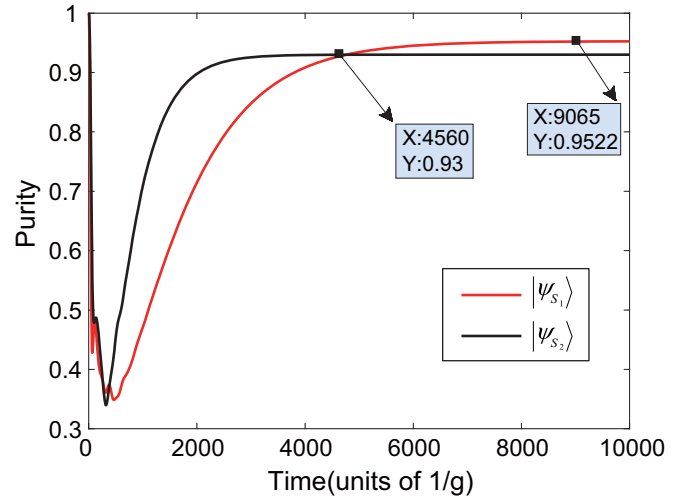

FIG. 4. Purities as a function of evolution time for the $|\psi_{S_1}\rangle$ and $|\psi_{S_2}\rangle$ with the initial state $|gg\rangle$. The systemic parameters corresponding to the $|\psi_{S_1}\rangle$ and $|\psi_{S_2}\rangle$ are the same as those in Figs. 3(a) and 3(b), respectively.

modulated with systematic parameters Ω_L and β. Dissipative processes generally lead to the production of mixed states. Therefore, we introduce purity to characterize the mixture degree of the target state. In Fig. 4, the purities of the $|\psi_{S_1}\rangle$ (red solid line) and $|\psi_{S_2}\rangle$ (black solid line) are plotted as a function of the evolution time. Owing to the initial state of the system being $|gg\rangle$, the purity is precisely unity. In addition, note that the purity curves exhibit a valley in the regime $0 < t < 1000/g$. This valley occurs because the coherent driving is dominant in the early stages of evolution, thus leading the system to be in a mixture of a variety of quantum states. With increasing evolution time, the competition between the coherent driving and dissipation gradually drives the system to a dynamic equilibrium.

B. Use spontaneous emission of NV centers as a resource

In this subsection, aiming to gain better insight into the effect of spontaneous emission of NV centers on the preparation of entanglement, we consider a perfect resonator without decay. As shown in Fig. 5(a), $\hat{\mathcal{L}}_{\text{eff}}^{\gamma_1}$ [Eq. (B6) in Appendix B] indicates the states $|gg\rangle$, $|T\rangle$, and $|S\rangle$ with effective level shifts $\Gamma_{1,1}$, $\Gamma_{1,2}$ and $\Gamma_{1,3}$, respectively, and effective decays from $|T\rangle$ to $|S\rangle$ at a rate $\Gamma_{1,2}$ and from $|S\rangle$ to $|T\rangle$ at a rate $\Gamma_{1,3}$; $\hat{\mathcal{L}}_{\text{eff}}^{\gamma_3}$ [Eq. (B7) in Appendix B] denotes the effective decays from $|gg\rangle$ to $|T\rangle$ and $|S\rangle$ at a rate $\Gamma_{3,1}$, respectively, from $|T\rangle$ to $|ff\rangle$ at a rate $\Gamma_{3,2}$ and from $|S\rangle$ to $|ff\rangle$ at a rate $\Gamma_{3,3}$. The spontaneous emission rates $\Gamma_{1,\epsilon}$ and $\Gamma_{3,\epsilon}$ $(\epsilon = 1, 2, 3)$ are equal to the square of the ϵth coefficient on the right-hand side of Eqs. ((B6)) and (B7), respectively. If we set $\tilde{\Delta}_{1,\text{eff}} \simeq 0$,

$$J = \sqrt{\delta^2 - (\delta/\Delta)g^2} \qquad (12)$$

would be achieved, thus parameter relation $\Gamma_{1(3),1} \gg \Gamma_{1(3),2}$, $\Gamma_{1(3),3}$ is satisfied. The dominant decays from $|gg\rangle$ to $|S\rangle$ and $|T\rangle$ can both be largely enhanced. Two effective classical fields induce transitions between the three triplet states $\{|gg\rangle, |ff\rangle, |T\rangle\}$ and between triplet state $|T\rangle$ and the singlet
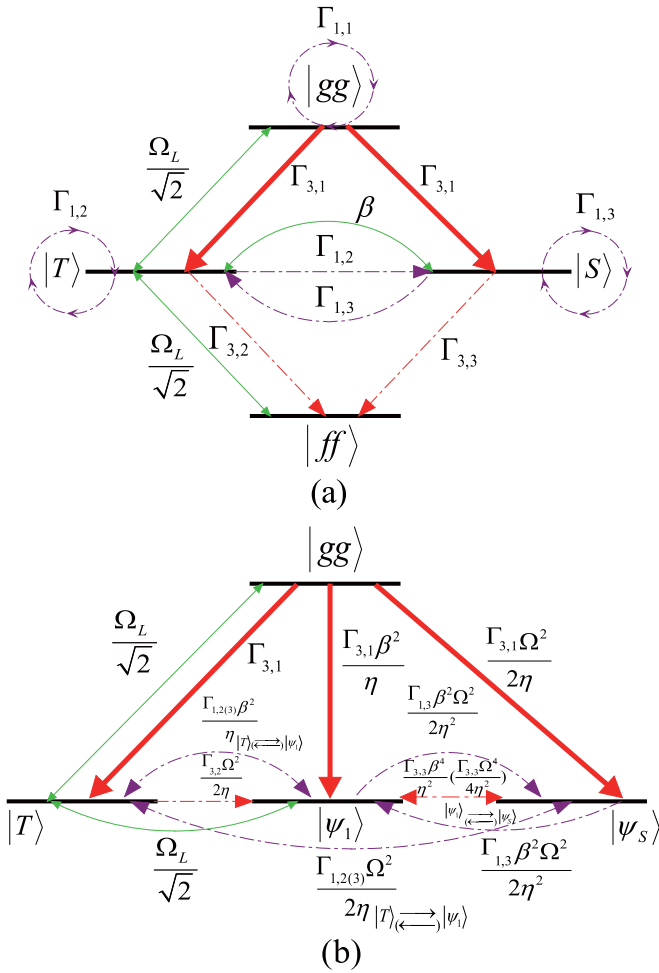
FIG. 5. Effective processes for coherent and dissipative (spontaneous emission of NV centers) interactions. (a) In the triplet-singlet basis picture, effective classical fields cause resonant transitions between the three triplet states $\{|gg\rangle, |ff\rangle, |T\rangle\}$. The singlet state $|S\rangle$ is coherently coupled to $|T\rangle$ by the level shift β. The states of the NV center decay from $|gg\rangle$ to $|S\rangle$ and $|T\rangle$ with effective decay rate $\Gamma_{3,1}$, and from $|T\rangle$ and $|S\rangle$ to $|ff\rangle$ with effective decay rates $\Gamma_{3,2}$ and $\Gamma_{3,3}$. The loop-like elements $\Gamma_{1,1}$, $\Gamma_{1,2}$, and $\Gamma_{1,3}$ represent the square of the coefficient in the corresponding term $|X\rangle\langle X|$ $(X = gg, T, S)$. (b) In the steady-state picture, the desired steady state $|\psi_S\rangle$ is no longer coherently coupled, but dissipatively prepared from $|gg\rangle$ at a rate of $\Gamma_{3,1}\Omega^2/2\eta$, where $\eta = \beta^2 + \Omega^2/2$.

state $|S\rangle$ [Eq. (B2) in Appendix B]. In this case, we can also prepare the steady state of the two NV centers in an entangled $|\psi_S\rangle$ state.

We move on to the steady state picture as shown in Fig. 5(b): the dissipation dynamics of the system is mainly governed by the effective decays from $|gg\rangle$ to $|\psi_S\rangle$ at a rate $\Gamma_{3,1}\Omega^2/2\eta$, from $|gg\rangle$ to $|\psi_1\rangle$ at a rate $\Gamma_{3,1}\beta^2/\eta$, and from $|gg\rangle$ to $|T\rangle$ at a rate $\Gamma_{3,1}$, where $\eta = \beta^2 + \Omega^2/2$. The effective decay channels related to $\Gamma_{1,2}$, $\Gamma_{1,3}$, $\Gamma_{3,2}$, and $\Gamma_{3,3}$ can be approximately ignored. With the coherent drivings and spontaneous emission of NV centers continuing, the population of the desired entangled state $|\psi_S\rangle$ is gradually accumulated over time for arbitrary initial state. In Figs. 6 and 7, we plot the fidelities and purities of target states $|\psi_{S_1}\rangle$ and $|\psi_{S_2}\rangle$

respectively, starting from the initial state $|gg\rangle$ with a set of optimal parameters. One can see that the desired states can be achieved with high fidelity and purity.
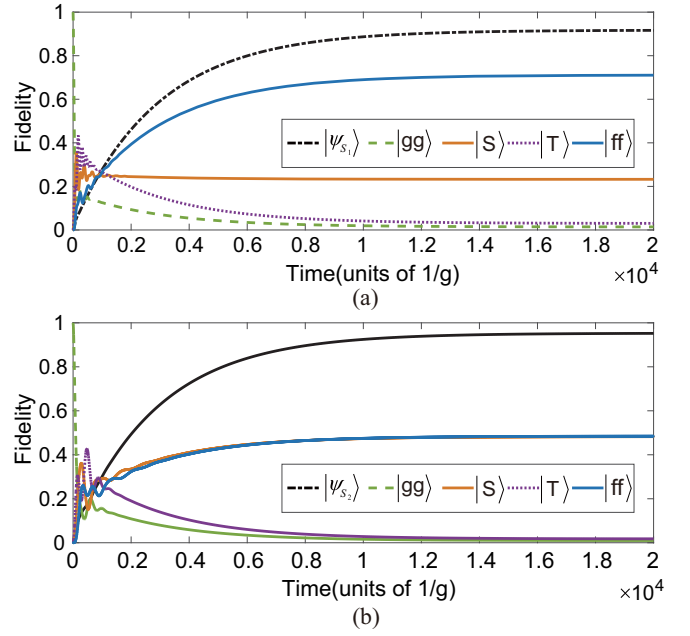

FIG. 6. (a) [(b)] Time evolution of the fidelities of target state $|\psi_{S_1}\rangle$ [$|\psi_{S_2}\rangle$], three triplet states $\{|gg\rangle, |ff\rangle, |T\rangle\}$, and singlet state $|S\rangle$ versus time in units of g^{-1} with the initial state $|gg\rangle$. In (a), the parameters are chosen as $\Omega = 0.085g$, $\Omega_L = 0.015g$, $\beta = 4\Omega_L/3$, $\Delta = 1.8g$, $\delta = 6.2g$, $J = \sqrt{\delta^2 - (\delta/\Delta)g^2}$, $\kappa = 0$, and $\gamma = 0.25g$. In (b), the parameters are chosen as $\Omega = 0.049g$, $\Omega_L = 0.007g$, $\beta = \Omega_L/\sqrt{2}$, $\Delta = 2g$, $\delta = 6.5g$, $J = \sqrt{\delta^2 - (\delta/\Delta)g^2}$, $\kappa = 0$, and $\gamma = 0.275g$.
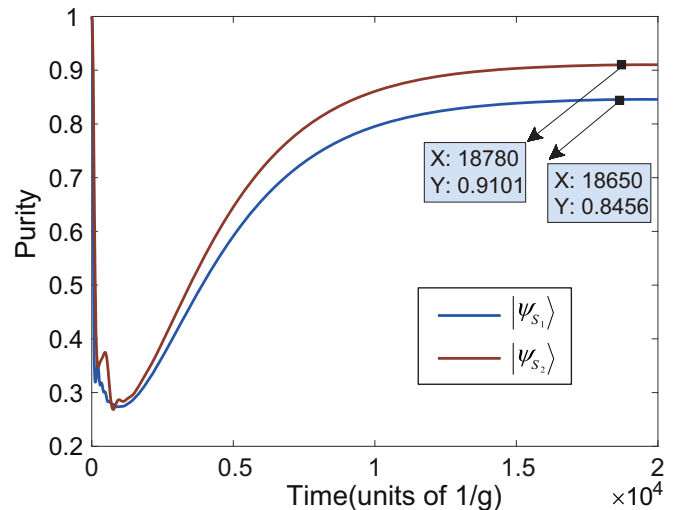

FIG. 7. Purities as a function of evolution time for the $|\psi_{S_1}\rangle$ and $|\psi_{S_2}\rangle$ with the initial state $|gg\rangle$. The systemic parameters corresponding to the $|\psi_{S_1}\rangle$ and $|\psi_{S_2}\rangle$ are the same as those in Figs. 6(a) and 6(b), respectively.
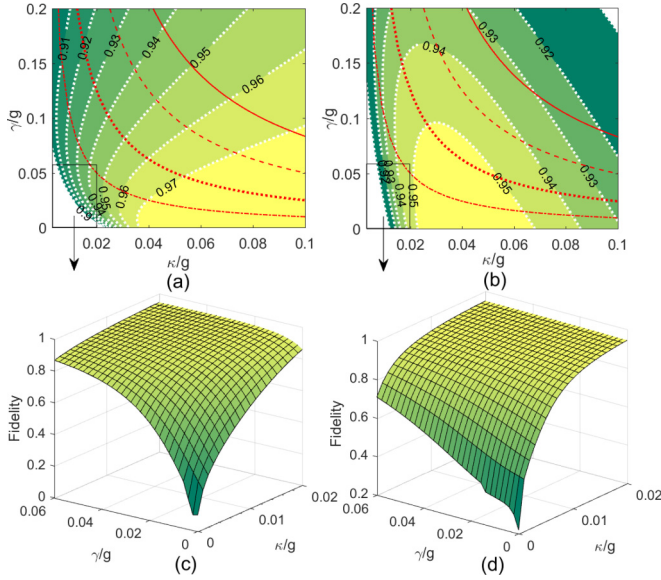
FIG. 8. [(a),(b)] Contour plot (white dotted lines) of steady state fidelity for the target states $|\psi_{S_1}\rangle$ and $|\psi_{S_2}\rangle$ versus spontaneous emission of NV centers γ/g and resonator decay κ/g with the initial state $|gg\rangle$. The red dash-dotted line, dotted line, dashed line, and solid line in (a) and (b) denote the cooperativity $C \equiv g^2/\kappa\gamma = 1000$, 400, 200, and 120 (from left to right), respectively. [(c),(d)] A three-dimensional plot correspond to the boxes in the bottom left corner of (a) and (b), in which γ/g and κ/g range from 0 to 0.06 and 0 to 0.02, respectively. In (a) and (c), the parameters are chosen as $\Omega = 0.075g$, $\Omega_L = 0.01g$, $\beta = 4\Omega_L/3$, $\Delta = 1.3g$, $\delta = 0.942g$, and $J = \sqrt{\delta^2 - (\delta/\Delta)g^2}$. In (b) and (d), the parameters are chosen as $\Omega_L = 0.015g$, $\beta = \Omega_L/\sqrt{2}$, $\Delta = 2.2g$, and other parameters are the same as in (a) and (c).

C. Use the two dissipative factors simultaneously to prepare the entangled state

From the above two subsections, we find that the parameter condition in Eq. (12) coincides with that in Eq. (9). It is thus possible to utilize both of these two dissipative factors simultaneously as resources for entanglement preparation. In that case, the effective decay processes can be characterized by $\hat{\mathcal{L}}_{\text{eff}}^{\kappa}$ and $\hat{\mathcal{L}}_{\text{eff}}^{\gamma}$ at the same time. By setting $M_{\kappa_1} = M_{\kappa_2} = \tilde{\Delta}_{1,\text{eff}} \simeq 0$, $J = \sqrt{\delta^2 - (\delta/\Delta)g^2}$ would be achieved, which leads to the effective decay rates $K_{1(2),1} \gg K_{1(2),2}$ and $\Gamma_{3,1} \gg \{\Gamma_{1,2}, \Gamma_{1,3}, \Gamma_{3,2}, \Gamma_{3,3}\}$, so that the effective decay channels caused by delocalized field modes decay $[|gg\rangle \rightarrow |\psi_1\rangle$ $(K_{1,1}\beta^2/\eta)$, $|gg\rangle \rightarrow |\psi_S\rangle$ $(K_{1,1}\Omega^2/2\eta)$, and $|gg\rangle \rightarrow |T\rangle$ $(K_{2,1})]$ and spontaneous emission of NV centers $[|gg\rangle \rightarrow |\psi_1\rangle$ $(\Gamma_{3,1}\beta^2/\eta)$, $|gg\rangle \rightarrow |\psi_S\rangle$ $(\Gamma_{3,1}\Omega^2/2\eta)$, and $|gg\rangle \rightarrow |T\rangle$ $(\Gamma_{3,1})]$ are greatly enhanced, while others are effectively suppressed, i.e., the engineered decays into state $|\psi_S\rangle$ are mediated to be much stronger than the decays out of $|\psi_S\rangle$. Consequently, the population of state $|\psi_S\rangle$ is accumulated asymptotically to a steady value with time. Furthermore, coherent coupling of the undesired states $|gg\rangle$, $|T\rangle$, and $|\psi_1\rangle$ by the effective classical field $\Omega_L/\sqrt{2}$ guarantees that the populations in the steady-state picture tend rapidly towards the target state $|\psi_S\rangle$.
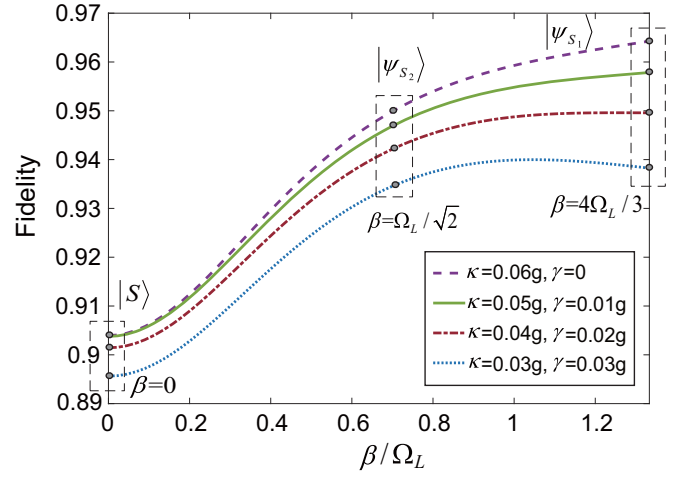

FIG. 9. Steady state fidelity for the target state $|\psi_S\rangle$ as a function of the ratio of systematic parameters β and Ω_L with different dissipative factors. Dashed boxes represent three specific values $\beta/\Omega_L = 0$, $1/\sqrt{2}$, and $4/3$ corresponding to the fidelity of states $|S\rangle$, $|\psi_{S_1}\rangle$, and $|\psi_{S_2}\rangle$, respectively. The remaining parameters are chosen as $\Omega = 0.05g$, $\Delta = 1.3g$, $\delta = 0.942g$, and $J = \sqrt{\delta^2 - (\delta/\Delta)g^2}$.

In Figs. 8(a) and 8(b), we plot the contour of the fidelity for target states $|\psi_{S_1}\rangle$ and $|\psi_{S_2}\rangle$ versus two dissipative factors after solving the master equation numerically, and we add four curves which denote that the cooperativity $C \equiv g^2/\kappa\gamma = 1000$ (red dash-dotted line), 400 (red dotted line), 200 (red dashed line), and 120 (red solid line) from left to right, respectively. The value of each corresponding cooperativity for the optimal fidelity of $|\psi_{S_1}\rangle$ $(|\psi_{S_2}\rangle)$ approaches 98.6% (95.7%), 98.3% (95.3%), 97.6% (94.4%), and 97.1% (93.3%), respectively. The results show that the fidelity of the desired stated would be higher than 90% even when the cooperativity C is as low as 200; these data are instrumental for researchers to seek more suitable physical systems for preparation of entanglement with high fidelity. The boxes in the bottom left corner of Figs. 8(a) and 8(b) correspond to the three-dimensional plots in Figs. 8(c) and 8(d) where the γ/g and κ/g range from 0 to 0.06 and from 0 to 0.02, respectively. One can see from Figs. 8(c) and 8(d) that, when the values of the dissipative factors are set to zero, the scheme will not succeed. As two dissipative factors increase, the role of the dissipative process becomes evident and the fidelity increases. Moreover, the results give a further verification that both of the dissipative factors could be utilized to prepare the desired steady state $|\psi_S\rangle$.

In addition, it is clear that the form of steady state $|\psi_S\rangle$ in Eq. (10) is related to the systematic parameters β and Ω_L. Therefore, we can prepare an entangled state with different forms on demand by modulating β/Ω_L. This distinct feature of the present scheme may find important applications in quantum information and quantum computation. To further demonstrate this point, in Fig. 9 we plot the fidelity of the target steady state as a function of the ratio β/Ω_L under the different dissipative factors and choose three values $\beta/\Omega_L = 0$, $1/\sqrt{2}$, and $4/3$ in the dashed boxes (from left to right), which correspond to Bell state $|S\rangle$, singlet-like state $|\psi_{S_2}\rangle$, and $|\psi_{S_1}\rangle$,
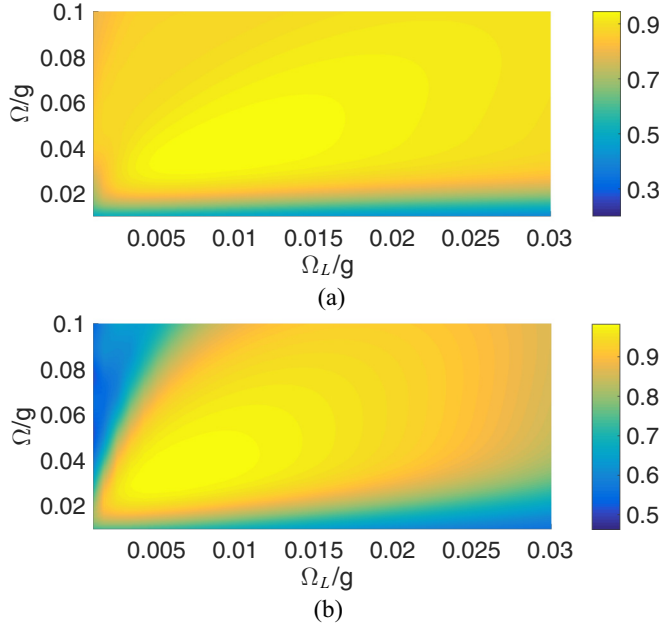
FIG. 10. Fidelities of the target steady states $|\psi_{S_1}\rangle$ and $|\psi_{S_2}\rangle$ as a function of the parameters Ω and Ω_L with the initial state $|gg\rangle$ at the times $2 \times 10^4/g$ and $1 \times 10^4/g$, respectively. In (a), the parameters are chosen as $\beta = 4\Omega_L/3$, $\Delta = 1.3g$, $\delta = 0.942g$, $J = \sqrt{\delta^2 - (\delta/\Delta)g^2}$, $\kappa = 0.05g$, and $\gamma = 0.1g$. In (b), the parameters are chosen as $\beta = \Omega_L/\sqrt{2}$, $\Delta = 2.2g$, $\delta = 0.942g$, $J = \sqrt{\delta^2 - (\delta/\Delta)g^2}$, $\kappa = 0.03g$, and $\gamma = 0.05g$.

respectively. It is also observed that the fidelity increases with the increase of β in a specific range.

IV. ROBUSTNESS OF SCHEME AND PRACTICAL CONSIDERATIONS

It is necessary to verify that the scheme is robust against moderate fluctuations of the systemic parameters through numerical simulations. In Figs. 10(a) and 10(b), the fidelities of target states $|\psi_{S_1}\rangle$ and $|\psi_{S_2}\rangle$ are plotted as functions of the Rabi frequencies Ω and Ω_L, respectively, for the given dissipative factors κ and γ, from which one can see that the fidelities are higher than 90%, respectively, within a wide range of Rabi frequencies, demonstrating that the scheme is insensitive to deviations of the controlled parameters Ω and Ω_L. Note that the above analysis has neglected the dephasing effect of the NV centers, however, which should be considered under realistic circumstances. In the following, this detrimental effect will be included in the numerical simulation. The Lindblad operators describing the dephasing of NV centers can be written as $\hat{\mathcal{L}}_{\gamma_{\Phi_1}} = \sqrt{\gamma_\phi/2}(|e\rangle_1\langle e| - |g\rangle_1\langle g|)$, $\hat{\mathcal{L}}_{\gamma_{\Phi_2}} = \sqrt{\gamma_\phi/2}(|e\rangle_2\langle e| - |g\rangle_2\langle g|)$, $\hat{\mathcal{L}}_{\gamma_{\Phi_3}} = \sqrt{\gamma_\phi/2}(|e\rangle_1\langle e| - |f\rangle_1\langle f|)$, and $\hat{\mathcal{L}}_{\gamma_{\Phi_4}} = \sqrt{\gamma_\phi/2}(|e\rangle_2\langle e| - |f\rangle_2\langle f|)$, where γ_ϕ is the dephasing rate of NV centers. In Figs. 11(a) and 11(b), we plot the respective fidelity of two special types of entangled singlet-like states $|\psi_{S_3}\rangle = 1/\sqrt{3}(|S\rangle + \sqrt{2}|ff\rangle)$ and $|\psi_{S_4}\rangle = 1/\sqrt{3}(|ff\rangle + \sqrt{2}|S\rangle)$ from initial state $1/2(|gg\rangle + |S\rangle + |T\rangle + |ff\rangle)$ by utilizing both spontaneous
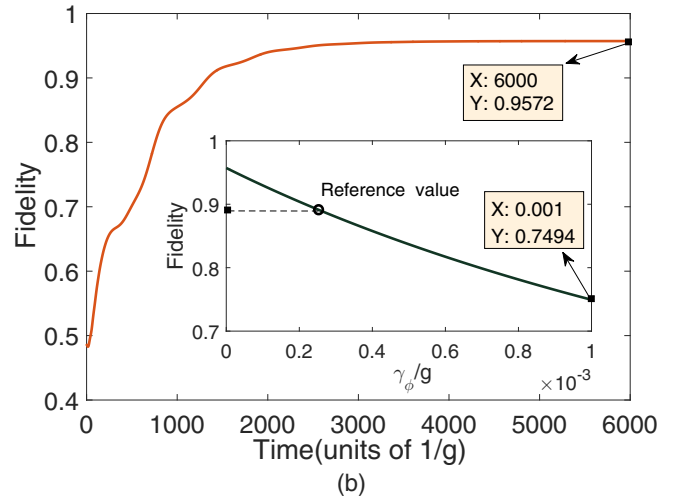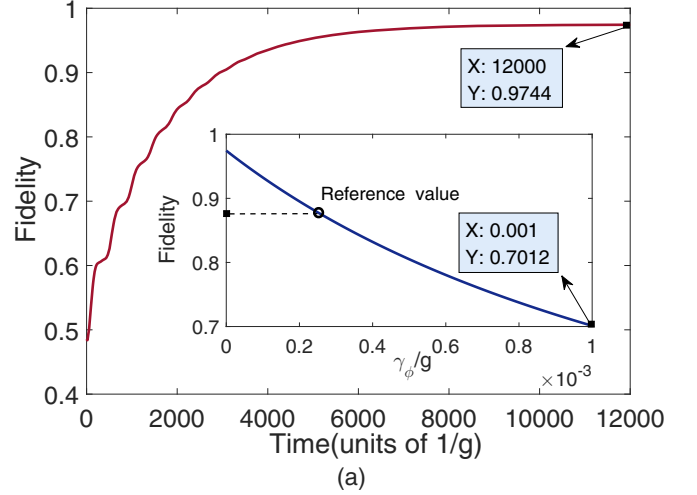

FIG. 11. (a) [(b)] Fidelity of a special type of entangled singlet-like state $|\psi_{S_3}\rangle = 1/\sqrt{3}(|S\rangle + \sqrt{2}|ff\rangle)[|\psi_{S_4}\rangle = 1/\sqrt{3}(|ff\rangle + \sqrt{2}|S\rangle)]$ as a function of evolution time with initial state $1/2(|gg\rangle + |S\rangle + |T\rangle + |ff\rangle)$. The parameters are chosen as $\Omega = 0.04g$, $\Omega_L = 0.01g$, $\beta = \Omega_L$, $\Delta = 1.5g$, $\delta = 0.942g$, $J = \sqrt{\delta^2 - (\delta/\Delta)g^2}$, $\kappa = 0.05g$, $\gamma = 0.04g$, and $\gamma_\phi = 0$ [$\beta = \Omega_L/2$ and other parameters are the same as in (a)]. The inset of (a) [(b)] shows the fidelity of the target steady state as a function of the dephasing rate of NV centers, γ_ϕ, which varies from 0 to 0.001 at time 2×10^4. The reference value of the fidelity corresponding to the dephasing rate of NV centers is $\gamma_\phi \simeq 2.653 \times 10^{-4}g$, which is an estimated value based on the experimental works [76,77].

emission of NV centers and delocalized field mode decay as resources without consideration of dephasing, from which we can see that the system evolves to the steady state with fidelities higher than 97% and 95%, respectively. In the inset of Fig. 11(a) [11(b)], we consider the system in stabilization and plot the fidelity versus the dephasing rate of NV centers, γ_ϕ. The fidelity is observed to decrease as γ_ϕ increases. Experimentally, the dephasing time induced by the nearby nuclear spin can reach about 2 ms with an isotopically pure diamond sample [76] and the NV centers are coupled with a chip-based microcavity with quality factor $Q > 25\,000$, and the coupling strength between a single microdisk photon and
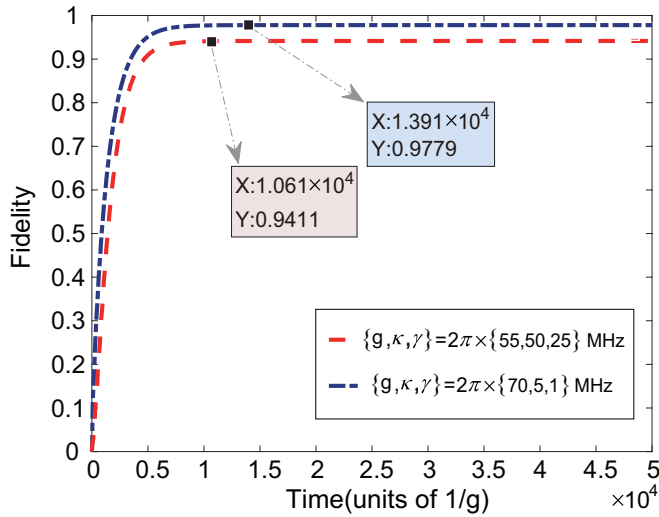
FIG. 12. Fidelity of $|\psi_{S_1}\rangle$ with two groups of experimental parameters versus time in units of g^{-1}. The red (dashed) and blue (dash-dotted) lines are plotted with the typical experimental parameters extracted from Refs. [77,84], respectively.

the NV center zero phonon line (ZPL) is $g/2\pi \sim 0.3$ GHz [77]. Taking the above factors into consideration, in our simulated data we choose $\gamma_\phi \simeq 2.653 \times 10^{-4}g$ as reference standard, which correspond to the fidelity 87.73% [89.13%]. When γ_ϕ changes from 0 to $2.653 \times 10^{-4}g$, the fidelity is decreased by 9.71% [6.59%]. This result occurs because the dephasing of NV centers results in a population transfer between the singlet states $|T\rangle$ and $|S\rangle$, decreasing the fidelity of the target state.

Our protocol is based on theoretical and realistic experimental progress, e.g., the optical Λ-type three-level structure in the NV center system [42,53–55] and the light-matter coherent coupling in quantized WGM resonators [45,77,78]. Technological advance has recently made it possible to realize strong coupling that depends on the critical photon number to saturate an NV qubit [79]. It requires the NV center to be embedded in an optical nanocavity with the evanescent field of the WGM, which is of importance because it offers an effective way to exchange energy between the WGM and the NV center, and significantly improves the resonant ZPL [80,81] relevant to the emitted photons from the NV centers. In the presence of a cavity, 70% of the photonic emission would be in the ZPL, and with an achievable collection efficiency of $\sim$90% [82]. Experimentally, the coupling strength between NV centers and the WGM can reach $g/2\pi \sim 0.3$–1 GHz [43,45,77,83]. We consider two sets of relevant attainable experimental cavity QED parameters $[(g, \kappa, \gamma)/2\pi = (55, 50, 25)$ MHz, $(70, 5, 1)$ MHz] extracted from Refs. [45,84]. The numerical results of our scheme are shown in Fig. 12. It is clearly seen that the fidelity of desired state $|\psi_{S_1}\rangle$ can reach 94.11% and 97.79% when the the time required for the system to reach the steady state is about 30.71 μs and 31.52 μs, respectively. The other parameters are chosen as $\Omega = 0.085g$, $\Omega_L = 0.015g$, $\beta = 4\Omega_L/3$, $\Delta = 1.8g$, $\delta = 6.2g$, and $J = \sqrt{\delta^2 - (\delta/\Delta)g^2}$. It is worth noting that the essential idea of the above discussions can be generalized to a system in which two microsphere resonators coupled

by an optical-fiber-taper waveguide, due to the near-perfect fiber-cavity coupling with an efficiency in excess of 99.97%, has been achieved using fiber-taper coupling to high-Q silica microspheres [48]. The optical fiber decay at 852 nm wavelength is about 2.2 dB/km [85], leading to fiber decay rates $\kappa_f = 0.152$ MHz.

On the other hand, the main parameters of decoherence are characterized by spin relaxation time and dephasing time. As discussed in [83], the electron spin relaxation time of NV centers in diamond scales from $\sim$ms at room temperature to $\sim$s at low temperature. The dephasing time induced by the nearby nuclear-spin fluctuation of more than 600 μs for the spin ensemble has been demonstrated [86]. According to the numerical results in our scheme, the time to reach the steady state $|\psi_S\rangle$ is about $10^4/g \simeq 5.3$ μs, which is shorter than the typical decoherence time for this system. Moreover, note that identical NV centers are required in our proposal; although it is a challenge with current techniques, the energy levels of different NV centers can be adjusted by external magnetic fields. Therefore, even though experimental imperfections exist, our scheme still has a certain experimental feasibility.

V. CONCLUSION

In conclusion, we have proposed a scheme for dissipative preparation of a KLM-type steady entangled state of two spatially separated NV centers based on the effective operator method. Spontaneous emission of NV centers and resonator decay have been investigated to achieve the desired state, consecutively and simultaneously. The whole evolution process leads to the population moving into and out of the target state, so that it is the steady state of the system. We have shown that entanglement can be obtained with high fidelity and purity regardless of the initial state, and that it is robust against parameter fluctuations. Considering current technologies and the future technical advances, we hope that this work will be useful in future applications of distributed quantum communication and quantum computation with solid-state cavity QED system.

APPENDIX A: EFFECTIVE GROUND STATE COUPLING VIA TWO-PHOTON RAMAN PROCESS

In order to realize the effective coupling between ground state sublevels $|m_s = +1\rangle$ and $|m_s = -1\rangle$, we consider a two-photon Raman process for the electronic ground states of NV1 and NV2. As illustrated in Fig. 13(a) [13(b)], two additional lasers are employed to drive the transitions $|0\rangle_{1(2)} \leftrightarrow |g\rangle_{1(2)}$ and $|0\rangle_{1(2)} \leftrightarrow |f\rangle_{1(2)}$ with Rabi frequencies $\Omega'_{1(3)}$ and $\Omega'_{2(4)}$, detunings $\Delta_{1(2)}$ and $\Delta_{2(1)}$, respectively. The time-dependent
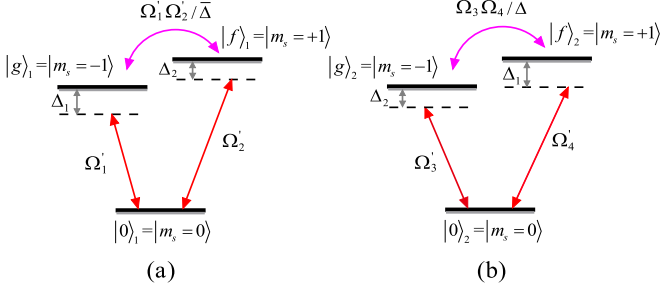
FIG. 13. Level structure of NV1 (a) and NV2 (b) in the electronic ground states $|^3A_2\rangle$. The qubits $|0\rangle$, $|g\rangle$, and $|f\rangle$ are encoded into the spin states $|m_s = 0\rangle$, $|m_s = -1\rangle$, and $|m_s = +1\rangle$, respectively. Two external laser fields are applied to dispersively drive NV1 and NV2, respectively, which induce an effective coupling between ground state sublevels $|m_s = +1\rangle$ and $|m_s = -1\rangle$.

interaction Hamiltonian in the interaction picture is

$$
\begin{aligned}
H_I &= \Omega_1' |g\rangle_1 \langle 0| e^{i\Delta_1 t} + \Omega_2' |f\rangle_1 \langle 0| e^{i\Delta_2 t} \\
&\quad + \Omega_3' |g\rangle_2 \langle 0| e^{i\Delta_2 t} + \Omega_4' |f\rangle_2 \langle 0| e^{i\Delta_1 t} + \text{H.c.,}
\end{aligned} \quad \text{(A1)}
$$

under the large-detuning conditions $\Delta_1 \gg \{\Omega_1', \Omega_4'\}$, $\Delta_2 \gg \{\Omega_2', \Omega_3'\}$, we obtain an effective Hamiltonian by utilizing the method proposed in [87],

$$
\begin{aligned}
H_{\text{eff}} &= \frac{\Omega_1'^2}{\Delta_1}(|g\rangle_1 \langle g| - |0\rangle_1 \langle 0|) + \frac{\Omega_2'^2}{\Delta_2}(|f\rangle_1 \langle f| - |0\rangle_1 \langle 0|) \\
&\quad + \frac{\Omega_3'^2}{\Delta_2}(|g\rangle_2 \langle g| - |0\rangle_2 \langle 0|) + \frac{\Omega_4'^2}{\Delta_1}(|f\rangle_2 \langle f| - |0\rangle_2 \langle 0|) \\
&\quad + \left(\frac{\Omega_1' \Omega_2'}{\bar{\Delta}} |g\rangle_1 \langle f| e^{i(\Delta_1 - \Delta_2)t} \right. \\
&\quad \left. + \frac{\Omega_3' \Omega_4'}{\bar{\Delta}} |g\rangle_2 \langle f| e^{-i(\Delta_1 - \Delta_2)t} + \text{H.c.} \right),
\end{aligned} \quad \text{(A2)}
$$

where $\bar{\Delta} = 2\Delta_1 \Delta_2 / (\Delta_1 + \Delta_2)$; in the rotating frame with $U \equiv \Omega_1'^2/\Delta_1(|g\rangle_1\langle g| - |0\rangle_1\langle 0|) + \Omega_2'^2/\Delta_2(|f\rangle_1\langle f| - |0\rangle_1\langle 0|) + \Omega_3'^2/\Delta_2(|g\rangle_2\langle g| - |0\rangle_2\langle 0|) + \Omega_4'^2/\Delta_1(|f\rangle_2\langle f| - |0\rangle_2\langle 0|)$, the effective Hamiltonian becomes

$$
\begin{aligned}
H_{\text{eff}}' &= \left(\frac{\Omega_1' \Omega_2'}{\bar{\Delta}} |g\rangle_1 \langle f| e^{i(\Delta_1 - \Delta_2 + \frac{\Omega_1'^2}{\Delta_1} - \frac{\Omega_2'^2}{\Delta_2})t} \right. \\
&\quad \left. + \frac{\Omega_3' \Omega_4'}{\bar{\Delta}} |g\rangle_2 \langle f| e^{-i(\Delta_1 - \Delta_2 - \frac{\Omega_3'^2}{\Delta_2} + \frac{\Omega_4'^2}{\Delta_1})t} + \text{H.c.} \right),
\end{aligned} \quad \text{(A3)}
$$

and we tune the Rabi frequencies $\Omega_1' = \Omega_4'$ and $\Omega_2' = \Omega_3'$. In the original picture with respect to $U' = -(\Delta_1 - \Delta_2 + \Omega_1'^2/\Delta_1 - \Omega_2'^2/\Delta_2)(|f\rangle_1\langle f| - |f\rangle_2\langle f|)$, the effective Hamiltonian is described as

$$
\begin{aligned}
H_{\text{eff}}'' &= \left(\Delta_1 - \Delta_2 + \frac{\Omega_1'^2}{\Delta_1} - \frac{\Omega_2'^2}{\Delta_2} \right)(|f\rangle_1 \langle f| - |f\rangle_2 \langle f|) \\
&\quad + \left[\frac{\Omega_1' \Omega_2'}{\bar{\Delta}}(|g\rangle_1 \langle f| + |g\rangle_2 \langle f|) + \text{H.c.} \right],
\end{aligned} \quad \text{(A4)}
$$

and the corresponding parameters in Eq. (2) are as follows:

$$
\beta = \Delta_1 - \Delta_2 + \frac{\Omega_1'^2}{\Delta_1} - \frac{\Omega_2'^2}{\Delta_2},
$$

$$
\Omega_{L_1} = \Omega_{L_2} = \frac{\Omega_1' \Omega_2'}{\bar{\Delta}}. \quad \text{(A5)}
$$

APPENDIX B: EFFECTIVE HAMILTONIAN AND LINDBLAD OPERATORS

According to Eq. (8), the effective Hamiltonian, along with Lindblad operators corresponding to delocalized field mode decay can be derived as

$$
\begin{aligned}
\hat{H}_{\text{eff}} &= -\text{Re}\left[\frac{\Omega^2}{2\tilde{\Delta}_{1,\text{eff}}}\right]|gg\rangle\langle gg| - \text{Re}\left[\frac{\Omega^2}{4\tilde{\Delta}_{2,\text{eff}}}\right]|T\rangle\langle T| \\
&\quad - \text{Re}\left[\frac{\Omega^2}{4\tilde{\Delta}_{3,\text{eff}}}\right]|S\rangle\langle S| + \hat{H}_g,
\end{aligned} \quad \text{(B1)}
$$

in which

$$
\begin{aligned}
\hat{H}_g &= -\beta(|S\rangle\langle T| + |T\rangle\langle S|) + \frac{\Omega_L}{\sqrt{2}}(|gg\rangle\langle T| \\
&\quad + |T\rangle\langle ff|) + \text{H.c.,}
\end{aligned} \quad \text{(B2)}
$$

$$
\hat{\mathcal{L}}_{\text{eff}}^{\kappa_1} = \sqrt{\frac{(\delta + J)g_{\text{eff}}^2 \kappa/4}{M_{\kappa 1}^2 + N_{\kappa 1}^2}}|S\rangle\langle gg| + \sqrt{\frac{g_{\text{eff}}^2 \kappa/4}{P_{\kappa 1}^2 + Q_{\kappa 1}^2}}|ff\rangle\langle S|,
$$

$$
\quad \text{(B3)}
$$

$$
\hat{\mathcal{L}}_{\text{eff}}^{\kappa_2} = \sqrt{\frac{(\delta - J)g_{\text{eff}}^2 \kappa/4}{M_{\kappa 2}^2 + N_{\kappa 2}^2}}|T\rangle\langle gg| + \sqrt{\frac{g_{\text{eff}}^2 \kappa/4}{P_{\kappa 2}^2 + Q_{\kappa 2}^2}}|ff\rangle\langle T|,
$$

$$
\quad \text{(B4)}
$$

where

$$
\frac{1}{\tilde{\Delta}_{1,\text{eff}}} = \frac{-(\delta' - J)(\delta' + J)}{\delta' g^2 - \Delta'(\delta' - J)(\delta' + J)},
$$

$$
\frac{1}{\tilde{\Delta}_{2,\text{eff}}} = \frac{-gJ - \delta' g^2 + \Delta'(\delta' - J)(\delta' + J)}{[g^2 - \Delta'(\delta' - J)][g^2 - \Delta'(\delta' + J)]},
$$

$$
\frac{1}{\tilde{\Delta}_{3,\text{eff}}} = \frac{gJ - \delta' g^2 + \Delta'(\delta' - J)(\delta' + J)}{[g^2 - \Delta'(\delta' - J)][g^2 - \Delta'(\delta' + J)]},
$$

$$
M_{\kappa 1} = M_{\kappa 2} = \frac{\delta g^2}{\Delta} - (\delta^2 - J^2),
$$

$$
N_{\kappa 1} = N_{\kappa 2} = \kappa\left(\delta - \frac{g^2}{2\Delta}\right) + \frac{\gamma(\delta^2 - J^2)}{2\Delta},
$$

$$
P_{\kappa 1} = \frac{g^2}{\Delta} - (\delta - J), \quad Q_{\kappa 1} = \frac{\kappa}{2} + \frac{\gamma(\delta - J)}{2\Delta},
$$

$$
P_{\kappa 2} = \frac{g^2}{\Delta} - (\delta + J), \quad Q_{\kappa 2} = \frac{\kappa}{2} + \frac{\gamma(\delta + J)}{2\Delta},
$$

$$
g_{\text{eff}} = \frac{g\Omega}{\Delta}, \quad \delta' = \delta - \frac{i}{2}\kappa, \quad \Delta' = \Delta - \frac{i}{2}\gamma. \quad \text{(B5)}
$$

Under the weak driving condition, i.e., Ω is very small, the terms consisting of Ω^2 can be neglected in Eq. (B1), so that $\hat{H}_{\text{eff}} \simeq \hat{H}_g$. There are two primarily effective decay channels characterized by $\hat{\mathcal{L}}_{\text{eff}}^{\kappa_1}$ and $\hat{\mathcal{L}}_{\text{eff}}^{\kappa_2}$ through two delocalized

bosonic modes c_1 and c_2, respectively. We assume $\{\kappa, \gamma\} \ll \{g, \delta, J, \Delta\}$, so that the minor terms with higher order than κ^2, γ^2, and $\kappa\gamma$ in the denominators of $\hat{\mathcal{L}}_{\text{eff}}^{\kappa_1}$ and $\hat{\mathcal{L}}_{\text{eff}}^{\kappa_2}$ can be omitted.

Applying Eq. (8) again, the analytic expressions of spontaneous emissions of NV centers with the effective Lindblad operators $\hat{\mathcal{L}}_{\text{eff}}^{\gamma_1}$ and $\hat{\mathcal{L}}_{\text{eff}}^{\gamma_3}$ are given by

$$\hat{\mathcal{L}}_{\text{eff}}^{\gamma_1} = \sqrt{\frac{\gamma}{2}} \left[\frac{\Omega}{2} \left| \frac{1}{\tilde{\Delta}_{1,\text{eff}}} \right| |gg\rangle\langle gg| + \frac{\Omega}{4} \left| \frac{1}{\tilde{\Delta}_{2,\text{eff}}} \right| (|T\rangle\langle T| + |S\rangle\langle T|) \right.$$
$$\left. + \frac{\Omega}{4} \left| \frac{1}{\tilde{\Delta}_{3,\text{eff}}} \right| (|T\rangle\langle S| + |S\rangle\langle S|) \right], \tag{B6}$$

$$\hat{\mathcal{L}}_{\text{eff}}^{\gamma_3} = \sqrt{\frac{\gamma}{2}} \left[\frac{\Omega}{2\sqrt{2}} \left| \frac{1}{\tilde{\Delta}_{1,\text{eff}}} \right| (|T\rangle\langle gg| + |S\rangle\langle gg|) + \frac{\Omega}{2\sqrt{2}} \right.$$
$$\left. \times \left(\left| \frac{1}{\tilde{\Delta}_{2,\text{eff}}} \right| |ff\rangle\langle T| + \left| \frac{1}{\tilde{\Delta}_{3,\text{eff}}} \right| |ff\rangle\langle S| \right) \right], \tag{B7}$$

where $|\cdot|$ denotes modulus of the symbol in it, $\hat{\mathcal{L}}_{\text{eff}}^{\gamma_2} = \hat{\mathcal{L}}_{\text{eff}}^{\gamma_1}$, and $\hat{\mathcal{L}}_{\text{eff}}^{\gamma_4} = \hat{\mathcal{L}}_{\text{eff}}^{\gamma_3}$. For the sake of simplicity, we only explain the dissipative processes characterized by $\hat{\mathcal{L}}_{\text{eff}}^{\gamma_1}$ and $\hat{\mathcal{L}}_{\text{eff}}^{\gamma_3}$.

[1] A. R. Calderbank and P. W. Shor, Good quantum error-correcting codes exist, Phys. Rev. A **54**, 1098 (1996).

[2] *Quantum Error Correction*, edited by D. A. Lidar and T. Brun (Cambridge University Press, Cambridge, UK, 2013).

[3] L. M. Duan and G. C. Guo, Preserving Coherence in Quantum Computation by Pairing Quantum Bits, Phys. Rev. Lett. **79**, 1953 (1997).

[4] P. Zanardi, and M. Rasetti, Noiseless Quantum Codes, Phys. Rev. Lett. **79**, 3306 (1997).

[5] D. A. Lidar, I. L. Chuang, and K. B. Whaley, Decoherence-Free Subspaces for Quantum Computation, Phys. Rev. Lett. **81**, 2594 (1998).

[6] P. Zanardi, Stabilizing quantum information, Phys. Rev. A **63**, 012301 (2000).

[7] L. Viola, E. M. Fortunato, M. A. Pravia, E. Knill, R. Laflamme, and D. G. Cory, Experimental realization of noiseless subsystems for quantum information processing, Science **293**, 2059 (2001).

[8] F. Verstraete, M. M. Wolf, and J. I. Cirac, Quantum computation and quantum-state engineering driven by dissipation, Nat. Phys. **5**, 633 (2009).

[9] K. G. H. Vollbrecht, C. A. Muschik, and J. I. Cirac, Entanglement Distillation by Dissipation and Continuous Quantum Repeaters, Phys. Rev. Lett. **107**, 120502 (2011).

[10] F. Pastawski, L. Clemente, and J. I. Cirac, Quantum memories based on engineered dissipation, Phys. Rev. A **83**, 012304 (2011).

[11] J. T. Barreiro, M. Müller, P. Schindler, D. Nigg, T. Monz, M. Chwalla, M. Hennrich, C. F. Roos, P. Zoller, and R. Blatt, An open-system quantum simulator with trapped ions, Nature (London) **470**, 486 (2011).

[12] M. Müller, K. Hammerer, Y. L. Zhou, C. F. Roos, and P. Zoller, Simulating open quantum systems: From many-body interactions to stabilizer pumping, New J. Phys. **13**, 085007 (2011).

[13] M. B. Plenio, S. F. Huelga, A. Beige, and P. L. Knight, Cavity-loss-induced generation of entangled atoms, Phys. Rev. A **59**, 2468 (1999).

[14] S. Clark, A. Peng, M. Gu, and S. Parkins, Unconditional Preparation of Entanglement between Atoms in Cascaded Optical Cavities, Phys. Rev. Lett. **91**, 177901 (2003)

[15] M. J. Kastoryano, F. Reiter, and A. S. Sørensen, Dissipative Preparation of Entanglement in Optical Cavities, Phys. Rev. Lett. **106**, 090502 (2011).

[16] J. Busch, S. De, S. S. Ivanov, B. T. Torosov, T. P. Spiller, and A. Beige, Cooling atom-cavity systems into entangled states, Phys. Rev. A **84**, 022316 (2011).

[17] F. Reiter and A. S. Sørensen, Effective operator formalism for open quantum systems, Phys. Rev. A **85**, 032111 (2012).

[18] L. T. Shen, X. Y. Chen, Z. B. Yang, H. Z. Wu, and S. B. Zheng, Steady-state entanglement for distant atoms by dissipation in coupled cavities, Phys. Rev. A **84**, 064302 (2011).

[19] F. Reiter, M. J. Kastoryano, and A. S. Sørensen, Driving two atoms in an optical cavity into an steady entangled state using engineered decay, New J. Phys. **14**, 053022 (2012).

[20] X. Q. Shao, T. Y. Zheng, C. H. Oh, and S. Zhang, Dissipative creation of three-dimensional entangled state in optical cavity via spontaneous emission, Phys. Rev. A **89**, 012319 (2014).

[21] W. Qin, A. Miranowicz, P. B. Li, X. Y. Lü, J. Q. You, and F. Nori, Exponentially Enhanced Light-Matter Interaction, Cooperativities, and Steady-State Entanglement using Parametric Amplification, Phys. Rev. Lett. **120**, 093601 (2018).

[22] P. B. Li, S. Y. Gao, H. R. Li, S. L. Ma, and F. L. Li, Dissipative preparation of entangled states between two spatially separated nitrogen-vacancy centers, Phys. Rev. A **85**, 042306 (2012).

[23] S. B. Zheng and L. T. Shen, Generation and stabilization of maximal entanglement between two atomic qubits coupled to a decaying resonator, J. Phys. B: At. Mol. Opt. Phys. **47**, 055502 (2014); L. T. Shen, R. X. Chen, Z. B. Yang, H. Z. Wu, and S. B. Zheng, Preparation of two-qubit steady entanglement through driving a single qubit, Opt. Lett. **39**, 6046 (2014).

[24] S. L. Su, X. Q. Shao, H. F. Wang, and S. Zhang, Scheme for entanglement generation in an atom-cavity system via dissipation, Phys. Rev. A **90**, 054302 (2014).

[25] C. A. Muschik, E. S. Polzik, and J. I. Cirac, Dissipatively driven entanglement of two macroscopic atomic ensembles, Phys. Rev. A **83**, 052312 (2011).

[26] J. Cho, S. Bose, and M. S. Kim, Optical Pumping into Many-Body Entanglement, Phys. Rev. Lett. **106**, 020504 (2011).

[27] S. L. Su, Q. Guo, H. F. Wang, and S. Zhang, Simplified scheme for entanglement preparation with Rydberg pumping via dissipation, Phys. Rev. A **92**, 022328 (2015).

[28] X. Q. Shao, J. H. Wu, X. X. Yi, and G. L. Long, Dissipative preparation of steady Greenberger-Horne-Zeilinger states for Rydberg atoms with quantum Zeno dynamics, Phys. Rev. A **96**, 062315 (2017).

[29] S. Diehl, A. Micheli, A. Kantian, B. Kraus, H. P. Büchler, and P. Zoller, Quantum states and phases in driven open quantum systems with cold atoms, Nat. Phys. **4**, 878 (2008).

[30] A. Aspect, P. Grangier, and G. Roger, Experimental Realization of Einstein-Podolsky-Rosen-Bohm Gedankenexperiment: A New Violation of Bell's Inequalities, Phys. Rev. Lett. **49**, 91 (1982).

[31] R. Blatt and C. F. Roos, Quantum simulations with trapped ions, Nat. Phys. **8**, 277 (2012).

[32] S. L. Su, Y. Z. Tian, H. Z. Shen, H. P. Zang, E. J. Liang, and S. Zhang, Applications of the modifed Rydberg antiblockade regime with simultaneous driving, Phys. Rev. A **96**, 042335 (2017).

[33] S. L. Su, Y. Gao, E. J. Liang, and S. Zhang, Fast Rydberg antiblockade regime and its applications in quantum logic gates, Phys. Rev. A **95**, 022319 (2017); S. L. Su, H. Z. Shen, E. J. Liang, and S. Zhang, One-step construction of the multiple-qubit Rydberg controlled-PHASE gate, *ibid.* **98**, 032306 (2018).

[34] J. Hofmann, M. Krug, N. Ortegel, L. Gérard, M. Weber, W. Rosenfeld, and H. Weinfurter, Heralded entanglement between widely separated atoms, Science **337**, 72 (2012).

[35] G. Y. Chen, N. Lambert, C. H. Chou, Y. N. Chen, and F. Nori, Surface plasmons in a metal nanowire coupled to colloidal quantum dots: Scattering properties and quantum entanglement, Phys. Rev. B **84**, 045310 (2011).

[36] A. Wallraff, D. I. Schuster, A. Blais, L. Frunzio, R. S. Huang, J. Majer, S. Kumar, S. M. Girvin, and R. J. Schoelkopf, Strong coupling of a single photon to a superconducting qubit using circuit quantum electrodynamics, Nature (London) **431**, 162 (2004).

[37] K. Nagata, K. Kuramitani, Y. Sekiguchi, and H. Kosaka, Universal holonomic quantum gates over geometric spin qubits with polarised microwaves, Nat. Commun. **9**, 3227 (2018).

[38] F. Jelezko, T. Gaebel, I. Popa, M. Domhan, A. Gruber, and J. Wrachtrup, Observation of Coherent Oscillation of a Single Nuclear Spin and Realization of a Two-Qubit Conditional Quantum Gate, Phys. Rev. Lett. **93**, 130501 (2004).

[39] T. Gaebel, M. Domhan, I. Popa, C. Wittmann, P. Neumann, F. Jelezko, J. R. Rabeau, N. Stavrias, A. D. Greentree, S. Prawer, J. Meijer, J. Twamley, P. R. Hemmer, and J. Wrachtrup, Room-temperature coherent coupling of single spins in diamond, Nat. Phys. **2**, 408 (2006).

[40] C. G. Yale, B. B. Buckley, D. J. Christle, G. Burkard, F. J. Heremans, L. C. Bassett, and D. D. Awschalom, All-optical control of a solid-state spin using coherent dark states, Proc. Natl. Acad. Sci. USA **110**, 7595 (2013).

[41] C. Santori, P. Tamarat, P. Neumann, J. Wrachtrup, D. Fattal, R. Beausoleil, J. Rabeau, P. Olivero, A. Greentree, S. Prawer, F. Jelezko, and P. Hemmer, Coherent Population Trapping of Single Spins in Diamond under Optical Excitation, Phys. Rev. Lett. **97**, 247401 (2006).

[42] E. Togan, Y. Chu, A. S. Trifonov, L. Jiang, J. Maze, L. Childress, M. V. G. Dutt, A. S. Sørensen, P. R. Hemmer, A. S. Zibrov, and M. D. Lukin, Quantum entanglement between an optical photon and a solid-state spin qubit, Nature (London) **466**, 730 (2010).

[43] M. Larsson, K. N. Dinyari, and H. Wang, Composite optical microcavity of diamond nanopillar and silica microsphere, Nano Lett. **9**, 1447 (2009).

[44] W. L. Yang, Z. Q. Yin, Z. Y. Xu, M. Feng, and C. H. Oh, Quantum dynamics and quantum state transfer between separated nitrogen-vacancy centers embedded in photonic crystal cavities, Phys. Rev. A **84**, 043849 (2011).

[45] Y. S. Park, A. K. Cook, and H. Wang, Cavity QED with diamond nanocrystals and silica microspheres, Nano Lett. **6**, 2075 (2006).

[46] A. Young, C. Y. Hu, L. Marseglia, J. P. Harrison, J. L. O'Brien, and J. G. Rarity, Cavity enhanced spin measurement of the ground state spin of an NV center in diamond, New J. Phys. **11**, 013007 (2009).

[47] B. B. Buckley, G. D. Fuchs, L. C. Bassett, and D. D. Awschalom, Observation of spin-light coherence for single spin measurement and control in diamond, Science **330**, 1212 (2010).

[48] S. M. Spillane, T. J. Kippenberg, O. J. Painter, and K. J. Vahala, Ideality in a Fiber-Taper-Coupled Microresonator System for Application to Cavity Quantum Electrodynamics, Phys. Rev. Lett. **91**, 043902 (2003).

[49] K. J. Vahala, Optical microcavities, Nature (London) **424**, 839 (2003).

[50] Y. F. Xiao, C. L. Zou, B. B. Li, Y. Li, C. H. Dong, Z. F. Han, and Q. H. Gong, High-Q Exterior Whispering-Gallery Modes in a Metal-Coated Microresonator, Phys. Rev. Lett. **105**, 153902 (2010).

[51] D. W. Vernooy, A. Furusawa, N. P. Georgiades, V. S. Ilchenko, and H. J. Kimble, Cavity QED with high-Q whispering gallery modes, Phys. Rev. A **57**, R2293 (1998).

[52] W. L. Yang, Z. Y. Xu, M. Feng, and J. F. Du, Entanglement of separate nitrogen-vacancy centers coupled to a whispering-gallery mode cavity, New J. Phys. **12**, 113039 (2010).

[53] P. B. Li, S. Y. Gao, and F. L. Li, Quantum information transfer with nitrogen-vacancy centers coupled to a whispering-gallery microresonator, Phys. Rev. A **83**, 054306 (2011).

[54] W. L. Yang, Z. Q. Yin, Z. Y. Xu, M. Feng, and J. F. Du, One-step implementation of multiqubit conditional phase gating with nitrogen-vacancy centers coupled to a high-Q silica microsphere cavity, Appl. Phys. Lett. **96**, 241113 (2010).

[55] Q. Chen, W. L. Yang, M. Feng, and J. F. Du, Entangling separate nitrogen-vacancy centers in a scalable fashion via coupling to microtoroidal resonators, Phys. Rev. A **83**, 054305 (2011).

[56] W. F. Koehl, B. B. Buckley, F. J. Heremans, G. Calusine, and D. D. Awschalom, Room temperature coherent control of defect spin qubits in silicon carbide, Nature (London) **479**, 84 (2011).

[57] J. J. Pla, K. Y. Tan, J. P. Dehollain, W. H. Lim, J. J. L. Morton, D. N. Jamieson, A. S. Dzurak, and A. Morello, A single-atom electron spin qubit in silicon, Nature (London) **489**, 541 (2012).

[58] L. Childress, M. V. G. Dutt, J. M. Taylor, A. S. Zibrov, F. Jelezko, J. Wrachtrup, P. R. Hemmer, and M. D. Lukin, Coherent dynamics of coupled electron and nuclear spin qubits in diamond, Science **314**, 281 (2006).

[59] J. J. Pla, K. Y. Tan, J. P. Dehollain, W. H. Lim, J. J. L. Morton, F. A. Zwanenburg, D. N. Jamieson, A. S. Dzurak, and A. Morello, High-fidelity readout and control of a nuclear spin qubit in silicon, Nature (London) **496**, 334 (2013).

[60] P. C. Maurer, G. Kucsko, C. Latta, L. Jiang, N. Y. Yao, S. D. Bennett, F. Pastawski, D. Hunger, N. Chisholm, M. Markham, D. J. Twitchen, J. I. Cirac, and M. D. Lukin, Room-temperature quantum bit memory exceeding one second, Science **336**, 1283 (2012).

[61] F. Dolde, V. Bergholm, Y. Wang, I. Jakobi, B. Naydenov, S. Pezzagna, J. Meijer, F. Jelezko, P. Neumann, T. Schulte-Herbrüggen, J. Biamonte, and J. Wrachtrup, High-fidelity spin entanglement using optimal control, Nat. Commun. **5**, 3371 (2014).

[62] W. Pfaff, T. H. Taminiau, L. Robledo, H. Bernien, M. Markham, D. J. Twitchen, and R. Hanson, Demonstration of entanglement-by-measurement of solid-state qubits, Nat. Phys. **9**, 29 (2013).

[63] Q. Chen, I. Schwarz, and M. B. Plenio, Steady-state preparation of long-lived nuclear spin singlet pairs at room temperature, Phys. Rev. B **95**, 224105 (2017).

[64] D. D. B. Rao, S. Yang, and J. Wrachtrup, Dissipative entanglement of solid-state spins in diamond, Phys. Rev. A **95**, 022310 (2017).

[65] E. Knill, R. Laflamme, and G. J. Milburn, A scheme for efficient quantum computation with linear optics, Nature (London) **409**, 46 (2001).

[66] J. Modławska and A. Grudka, Nonmaximally Entangled States can be Better for Multiple Linear Optical Teleportation, Phys. Rev. Lett. **100**, 110503 (2008).

[67] J. Modławska and A. Grudka, Adaptive quantum teleportation, Phys. Rev. A **79**, 064302 (2009).

[68] J. R. Maze, A. Gali, E. Togan, Y. Chu, A. Trifonov, E. Kaxiras, and M. D. Lukin, Properties of nitrogen-vacancy centers in diamond: The group theoretic approach, New J. Phys. **13**, 025025 (2011).

[69] E. R. MacQuarrie, T. A. Gosavi, N. R. Jungwirth, S. A. Bhave, and G. D. Fuchs, Mechanical Spin Control of Nitrogen-Vacancy Centers in Diamond, Phys. Rev. Lett. **111**, 227602 (2013).

[70] N. B. Manson, J. P. Harrison, and M. J. Sellars, Nitrogen-vacancy center in diamond: Model of the electronic structure and associated dynamics, Phys. Rev. B **74**, 104303 (2006).

[71] A. Batalov, V. Jacques, F. Kaiser, P. Siyushev, P. Neumann, L. J. Rogers, R. L. McMurtrie, N. B. Manson, F. Jelezko, and J. Wrachtrup, Low Temperature Studies of the Excited-State Structure of Negatively Charged Nitrogen-Vacancy Color Centers in Diamond, Phys. Rev. Lett. **102**, 195506 (2009).

[72] J. Berezovsky, M. H. Mikkelsen, O. Gywat, N. G. Stoltz, L. A. Coldren, and D. D. Awschalom, Nondestructive optical measurements of a single electron spin in a quantum dot, Science **314**, 1916 (2006).

[73] M. Atatüre, J. Dreiser, A. Badolato, and A. Imamoglu, Observation of Faraday rotation from a single confined spin, Nat. Phys. **3**, 101 (2007).

[74] P. Tamarat, N. B. Manson, J. P. Harrison, R. L. McMurtrie, A. Nizovtsev, C. Santori, R. G. Beausoleil, P. Neumann, T. Gaebel, F. Jelezko, P. Hemmer, and J. Wrachtrup, Spin-flip and spin-conserving optical transitions of the nitrogen-vacancy centre in diamond, New J. Phys. **10**, 045004 (2008).

[75] X. T. Wang and S. G. Schirmer, Generating maximal entanglement between non-interacting atoms by collective decay and symmetry breaking, arXiv:1005.2114.

[76] G. Balasubramanian, P. Neumann, D. Twitchen, M. Markham, R. Kolesov, N. Mizuochi, J. Isoya, J. Achard, J. Beck, J. Tissler, V. Jacques, P. R. Hemmer, F. Jelezko, and J. Wrachtrup, Ultralong spin coherence time in isotopically engineered diamond, Nat. Mater. **8**, 383 (2009).

[77] P. E. Barclay, K. M. C. Fu, C. Santori, and R. G. Beausoleil, Chip-based microcavities coupled to nitrogenvacancy centers in single crystal diamond, Appl. Phys. Lett. **95**, 191115 (2009).

[78] S. Schietinger, T. Schröder, and O. Benson, One-by-one coupling of single defect centers in nanodiamonds to high-Q modes of an optical microresonator, Nano Lett. **8**, 3911 (2008).

[79] S. M. Spillane, T. J. Kippenberg, K. J. Vahala, K. W. Goh, E. Wilcut, and H. J. Kimble, Ultrahigh-*Q* toroidal microresonators for cavity quantum electrodynamics, Phys. Rev. A **71**, 013817 (2005).

[80] C. H. Su, A. D. Greentree, and L. C. L. Hollenberg, Towards a picosecond transform-limited nitrogen-vacancy based single photon source, Opt. Express **16**, 6240 (2008).

[81] J. Wolters, A. W. Schell, G. Kewes, N. Nüsse, M. Schoengen, H. Döscher, T. Hannappel, B. Löchel, M. Barth, and O. Benson, Enhancement of the zero phonon line emission from a single nitrogen vacancy center in a nanodiamond via coupling to a photonic crystal cavity, Appl. Phys. Lett. **97**, 141108 (2010).

[82] L. Li, E. H. Chen, J. Zheng, S. L. Mouradian, F. Dolde, T. Schröder, S. Karaveli, M. L. Markham, D. J. Twitchen, and D. Englund, Efficient photon collection from a nitrogen vacancy center in a circular bullseye grating, Nano Lett. **15**, 1493 (2015).

[83] P. E. Barclay, C. Santori, K. M. Fu, R. G. Beausoleil, and O. Painter, Coherent interference effects in a nano-assembled diamond NV center cavity-QED system, Opt. Express **17**, 8081 (2009).

[84] B. Dayan, A. S. Parkins, T. Aoki, E. P. Ostby, K. I. Vahala, and H. J. Kimble, A photon turnstile dynamically regulated by one atom, Science **319**, 1062 (2008).

[85] K. J. Gordon, V. Fernandez, P. D. Townsend, and G. S. Buller, A short wavelength gigahertz clocked fiber optic quantum key distribution system, IEEE J. Quantum Electron. **40**, 900 (2004).

[86] P. L. Stanwix, L. M. Pham, J. R. Maze, D. Le Sage, T. K. Yeung, P. Cappellaro, P. R. Hemmer, A. Yacoby, M. D. Lukin, and R. L. Walsworth, Coherence of nitrogen-vacancy electronic spin ensembles in diamond, Phys. Rev. B **82**, 201201 (2010).

[87] D. F. V. James and J. Jerke, Effective Hamiltonian theory and its applications in quantum information, Can. J. Phys. **85**, 625 (2007).